Stochastic study of stability of unsaturated heterogeneous slopes destabilised by rainfall

Thi Minh Hue Le

Norwegian Geotechnical Institute, Sognsveien 72, 0855 Oslo, Norway

1 Introduction

Understanding of unsaturated slope stability during rainfall infiltration is of critical importance in many parts of the world (e.g. southern Europe, Brazil, HongKong) where the hot climate give rise to extensive areas with unsaturated soils. On one hand, the unsaturated state actually improves slope stability in dry or partial saturation condition because the existence of suction (i.e. negative pore pressure) raises the soil strength compared with its saturated state. On the other hand, the diminish of the unsaturated condition due to, for example, wetting process by rainfall can lead to a reduction of the soil shear strength because of a reduction in suction and, possibly, a rise in positive pore water pressure. Both these effects directly contribute to destabilising unsaturated slopes. If porosity varies considerably in the soil mass, an extra level of complexity is added because the wetting front no longer migrates in a smooth and regular pattern over time as in a domain with uniform porosity. Instead, water follows atypical preferential paths causing uneven reduction of suction and, possibly, build-up of positive pore pressure in the soil masses. A soil element experiencing large suction loss might reach the failure condition earlier or under lower stresses than other neighboring elements experiencing a limited suction reduction. The slip surface then preferably passes through these failed elements despite having to follow an unusual shape. Heterogeneity of porosity can therefore alter the failure mechanism of an unsaturated slope subjected to rainfall.

Stability of a slope can normally be assessed using an analytical solution (for simple infinite slopes) or the traditional Limit Equilibrium Method (LEM) and/or the more advanced Finite Element Method (FEM). The FEM is often employed to deal with complex slope problems such as, for example, those having unusual geometries, subjected to complicated loading sequences, undergoing progressive failure or showing heterogeneous material properties. The problem considered in this study is rather complex and highly non-linear, hence the use of the FEM is necessary.

When it comes to probabilistic investigation of slope stability, most of studies reported in literature assumed that the slope is fully saturated (or fully dried). In many cases, the investigations focused on the spatial variability of shear strength, including undrained shear strength, or effective friction angle (ϕ') and/or effective cohesion (c'). Many past stochastic studies employ the Monte-Carlo approach due to its conceptual simplicity and its capability of handling complicated geometries and variability patterns without requiring over-simplified assumptions (e.g. [1-4]). Some studies demonstrated that the influence of soil heterogeneity on stability depend on various factors such as, for example, the slope characteristics (e.g. slope angle) or the combination of input parameters (e.g. mean and standard deviation of the random soil property).

Several studies have integrated the random field theory and the finite element method to model soil spatial variability. The method is often referred to as the "random finite element method" [1, 2, 5-9].

Past studies on unsaturated slope stability are almost exclusively limited to homogeneous soils. Griffiths and Lu (2005) [10] and Lu and Godt (2008) [11] devised a formula of suction stress which takes into account both soil characteristics and infiltration rate. The suction stress was then used to analytically predict the stability of an unsaturated slope in a steady seepage condition. A partially saturated slopes can also be analysed by the LEM in an uncoupled manner. This usually involves an independent flow analysis to obtain the pore water pressure distribution assuming rigid soil behaviour under given hydraulic boundary conditions. This pore water pressure distribution is then used as the groundwater condition to input into a subsequent limit equilibrium analysis [12].

This study investigates the stability of an unsaturated slope with spatially varying porosity using the random finite element method. The aim is to demonstrate the use of stochastic methods in investigating the risk associated with unsaturated soil heterogeneity at different points in time during and after a rainfall event. Particularly, the effects of soil variability (quantified by different values of the coefficient of variation) on the factor of safety of the slope are examined.

2 Methods

2.1 Slope geometry and boundary condition

This study investigates a slope is 10 m height, having an angle of 2:1 (or 26.6°) and resting on a base of 20 m thickness (Fig. 1). The initial stress distribution is in equilibrium with gravity (9.81 m^2/s) while the initial pore water pressure distribution is in hydrostatic equilibrium with the initial water table position at 5 m below the ground surface. The hydrostatic condition results in a maximum initial suction of approximately 150 kPa at the crest (AB) which falls in the low end of the prevalent surface suction range of semiarid or arid environments such as in Australia [13].

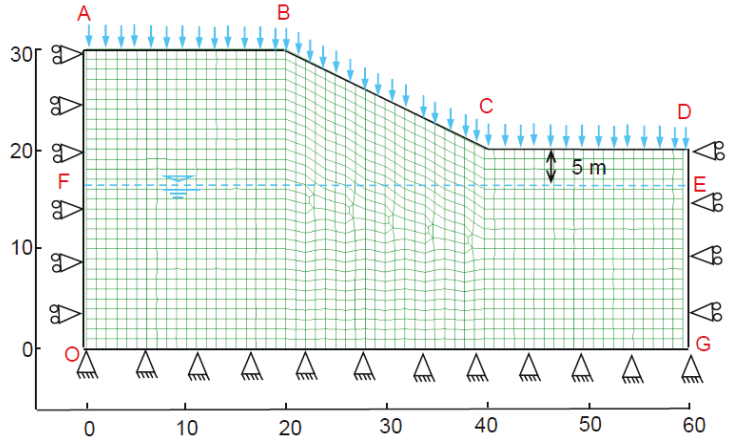

Figure 1: Slope dimensions, geometry and boundary conditions (scale in metre)

The slope is subjected to a rainfall event which extends continuously over 10 days after which the rainfall is terminated but the simulation was continued for another 355 days. The stability of the slope is assessed at different times both during and after the rainfall as explained in detail in subsequent sections. Rainfall is assumed to infiltrate into the slope through boundaries AB,

BC and CD over the ten days. These boundaries (AB, BC and CD) then become impermeable once the rainfall has stopped (i.e. day 10 onward). This means that there is no subsequent rainfall infiltration or evaporation at the ground surface, after the initial 10 days of rainfall. Boundaries DG, GO and OA are assumed to be impermeable both during and after the rainfall. The factor of safety are estimated at 0, 0.5, 5, 10, 15, 20, 100, 365 days from the starting time.

2.2 Hydraulic and mechanical models

The van Genuchten (1980) [14] and van Genuchten and Nielsen (1985) [15] water retention curve and permeability function are selected because they can represent the soil hydraulic behaviour in a simple and numerically stable way. Details of the selected hydraulic constitutive relationships can be found in Le *et al* (2015) [9]. The values of hydraulic parameters for the water retention curve and the permeability function are shown in Table 1. The main parameters are the reference saturated permeability, k_{so}, the reference air entry parameter, s_{eo}, the water retention curve gradient, m and the parameter controlling the dependency of water retention behaviour on porosity, η. In addition, the model requires input values of the maximum and minimum saturation, S_s and S_r, the reference porosity ϕ_o and the water density ρ_w. The values of the constitutive parameters are selected to be at around the middle of the likely range for each parameter in order to avoid overly large or small input parameters and, hence, possible unrepresentative or unrealistic results. For example, an extremely low permeability (i.e. very small k_{so}) would result in the rainfall having no effect on slope stability because water would not have sufficient time to infiltrate into the unsaturated soil domain. The rainfall intensity is assumed to be at 43.2 mm/day.

The extended Mohr - Coulomb model for unsaturated soils is selected to model failure behaviour [16]. The values adopted for the mechanical parameters are also shown in Table 1. These values are kept constant throughout the study. The typical property values of a clay are selected for the strength parameters (c', ϕ' and ϕ^b) and the elastic parameter, i.e. Young modulus (E) and Poisson ratio (ν).

Table 1: Values of hydraulic and mechanical soil parameters

Hydraulic			Mechanical		
Symbols	Units	Values	Symbols	Units	Values
m		0.2	E	kPa x 10^3	100
η		5	ν		0.3
ϕ_o		0.333	ϕ'	°	20
k_{so}	m/s	10^{-5}	c'	kPa	5
s_{eo}	kPa	20	ϕ^b	°	18
S_s		1	ρ_s	kg/m^3	2700
S_r		0.001			

The Factor of Safety (FoS) in the FEM is defined by relating the actual soil strength to the failure strength. In particular, the FoS is estimated in the FEM by inducing slope failure through a numerical process called shear strength reduction. This involves incrementally and continuously reducing the values of the shear strength parameters until instability is initiated. For unsaturated soil, Equation (1) is adopted in this study to conduct the shear strength reduction process which involves incremental reduction of $\tan\phi'$, c' and $\tan\phi^b$ [9, 17].

$$FoS = \frac{c'_{actual}}{c'_{fail}} = \frac{\tan\phi'_{actual}}{\tan\phi'_{fail}} = \frac{\tan\phi^{b}_{actual}}{\tan\phi^{b}_{fail}} \quad (1)$$

2.3 Random variable and random finite element method

Porosity is probably one of the most easily observed soil parameters which exhibit spatial variability. The variability characteristics of porosity have been investigated in a few studies (e.g. [18, 19]). In unsaturated soils, porosity variability leads to heterogeneity in the water retention behaviour and permeability of the soil [9, 20, 21]. During a rainfall event, infiltrated water is thus likely to follow unusual preferential flow paths in a porosity heterogeneous slope. Therefore, those soil elements subjected to an earlier or larger infiltration will loose the cohesive component of strength contributed by suction earlier than other soil elements or by a more substantial amount. This non-uniform strength reduction causes variation in the overall factor of safety.

In this study, the heterogeneity of porosity in each realization is created by generating first a random field of void ratio (e). Note that each "realization" refers to a deterministic distribution of porosity generated during Monte Carlo simulation. The e random field is modelled by a log-normal distribution which ensures that the generated random values are always positive. The values of ϕ calculated using $\phi = e/(1+e)$ are therefore always bounded between 0 and 1 as required. The values of mean $\mu(e)$ and correlation length $\theta(e)$ are kept constant at 0.5 and 8 m, respectively. A range of coefficient of variation, COV_e, between 0.1 and 1.6 are considered. This results in the corresponding values of $\mu(\phi)$ and COV_ϕ as presented in Table 2. As the COV_e increases at a constant $\mu(e)$, the $\mu(\phi)$ decreases while the COV_ϕ increases. The largest value of COV_ϕ are larger than the upper bound of the usual COV_ϕ range which can be found in, for example, Phoon *et al* (1999) [19] and Le *et al* [18]. The selection of such large values are to demonstrate the influence of porosity more clearly and to consider the extreme situation where such a large variability in porosity is possible (e.g. in fill materials).

Table 2: Parameters of porosity (ϕ) random field corresponding to different input values of COV_e and $\mu(e) = 0.5$

COV_e	0.1	0.2	0.4	0.8	1.6
$\mu(\phi)$	0.333	0.330	0.323	0.300	0.256
COV_ϕ	0.067	0.132	0.254	0.456	0.720

The same mesh of 1515 quadrilateral (squares or parallelograms) elements is employed consistently in every realization to eliminate undesired variations associated with mesh discretisations (Fig. 1). This mesh was shown to produce a reliable estimate of the factor of safety of homogeneous slope, which remained essentially unchanged for finer discretisations [9]. For each realisation, a random field with a grid of square cells is first generated with one random value allocated to each cell. A mapping process is then performed which involves superimposing the random field on the mesh. The superimposition allows to search and assign each finite element the random value from the cell having centroid closest to the centroid of the element. Each square element, and the vast majority of parallelogram elements, has an area of 1 m^2, with a few exceptions in the centre of the mesh. The relatively uniform sizes and similar shapes of the mesh elements ensure marginal discrepancy (caused the mapping procedure) between the variability characteristics of the random finite element mesh and the underlying random field.

An exemplary comparison between the statistics of the random variable mapped onto the mesh and the theoretical statistics is shown in Figure 2. The figure demonstrates that the probability density functions of both random field e and the mapped values of e on the finite element mesh are reasonably consistent with the theoretical probability distribution function (pdf) calculated from the input $\mu(e)$ and COV_e. The consistency however tends to deteriorate with increasing input COV_e. The corresponding random values of ϕ follows a pdf that appeared to be skewed-left and confined between 0 and 1.

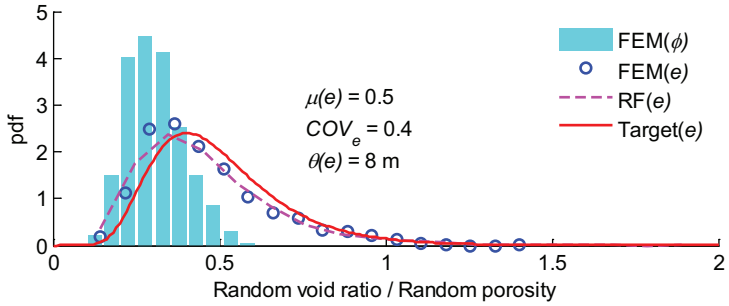

Figure 2: Histogram of a sample realization of random porosity mapped onto the mesh (FEM(ϕ)) and the pdf of associated void ratio (FEM(e)), of the underlying random void ratio field (RF(e)) and of the theoretical distribution generated from input parameters (Target(e))

3 Results and Discussions

3.1 Statistical characterisations

The main outputs of the Monte Carlo analysis in this study are the FoS. In order to be considered reliable, the statistics of the FoS should be stable with the number of realizations (i.e. do not change with more realizations). The convergences of the $\mu(FoS)$ and $\sigma(FoS)$ are assessed by plotting the evolution of mean with increasing number of realizations as, for example, shown in Figure 3. Individual data points and 95% confidence interval are also represented on these figures to indicate the range of variability, hence fluctuation of $\sigma(FoS)$. The $\mu(FoS)$ converges rather quickly after around 60 realizations. The 95% confidence interval also becomes relatively narrow after 60 realizations. A difference of approximately 0.06 is observed between the lower and upper bounds at this point indicating the stabilization of $\sigma(FoS)$. The FoS for individual realizations however spread over a reasonably wide range from just above 1 to just below 2 which is caused by the variation in suction distribution between individual realizations. Note that Figure 3 shows variation of data corresponds to 5 days of continous rainfall. Inspection of the results show that the FoS at this time (5 days) tends to be most varied. For other times, the convergence can be achieved with a lower number of realizations than 60.

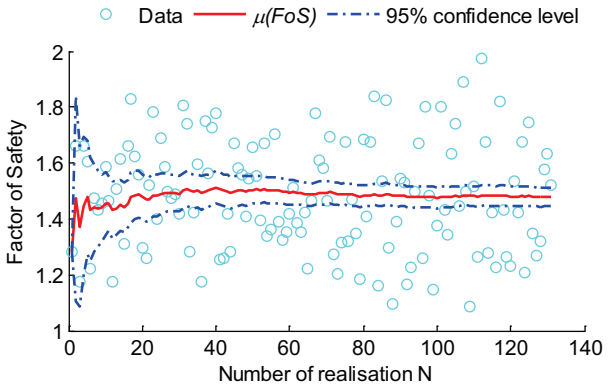

Figure 3: Convergence of FoS with the number of realizations (5 days, μ(e)= 0.5, COV_e = 0.8, θ(e) = 8 m)

Various techniques including visual observation of histograms, probability plots and chi squared goodness of fit tests are used to find the most suitable pdf to represent the distribution of the FoS data. It is found that the histograms of the FoS can be described reasonably well by the log-normal distribution function. As an example, the FoS histograms with their fitted log-normal pdfs at different times are shown in Figure 4 for different times.

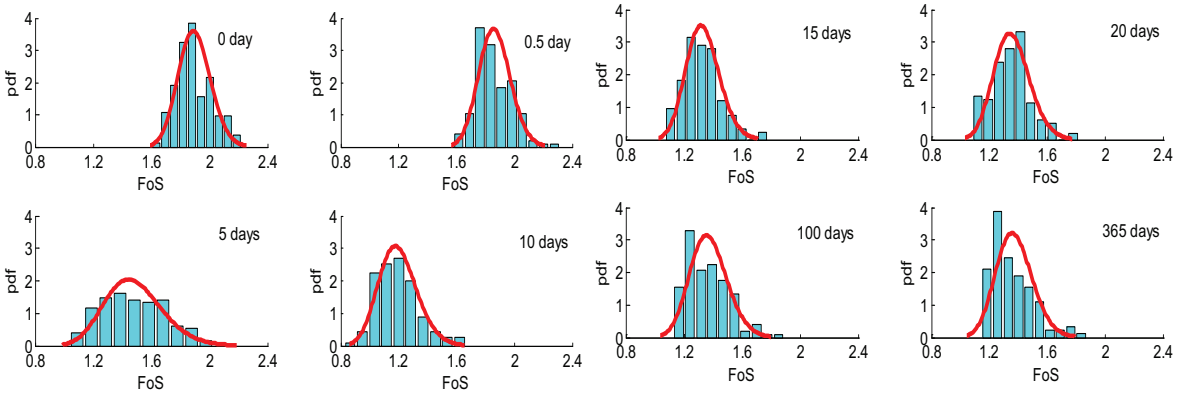

Figure 4: Histograms (bars) with the fitted log-normal distribution function (continuous line) of FoS at different times during the rainfall (μ(e)= 0.5, COV_e = 0.8, θ(e) = 8 m)

3.2 Failure mechanism during and after rainfall

A sample realization of random porosity is illustrated in Figure 5. The porosity values were calculated from the associated random field of *e* (COV_e = 0.8 and $\underline{\theta(e)}$ = 8 m) and mapped onto the finite element mesh (Fig. 5). The porosity value of the elements ranges between 0.05 to 0.75 which is a slightly large range compared with the typical range of porosity variation within a single domain of this size. The inclusion of such a large variation ranges is however considered reasonable in this study to highlight the effects of heterogeneity.

The changes in failure mechanism during and after a rainfall event due to the changes in suction and pore water pressure distribution are shown in Figure 6 (corresponding to porosity distribution shown in Fig. 5). The pore water pressure distributions are highly irregular at intermediate times from 5 to 20 days (Fig. 6). The FoS are lower while the sliding masses are also smaller (Fig. 6) at these times compared with other times. Conversely, the beginning (0 – 0.5 day) and the end (100 – 365 days) of the simulation period display less variability in the pore water pressure distribution and higher FoS. The area and depth of the failure masses at these times (0-0.5 or 100-365 days) are however significantly larger than at intermediate times (5-20 days).

The rise of the water table at the end of the simulation compared to the initial condition causes not only a drop in the FoS but also a reduction in the sliding mass size.

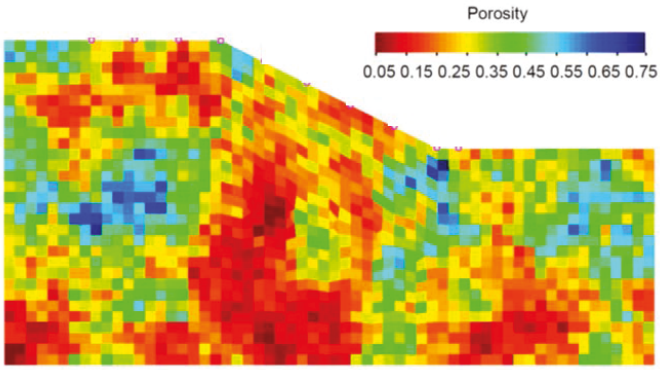

Figure 5: A typical realization of porosity distribution (transformed from the random void ratio field with $\mu(e)$ = 0.5, COV_e = 0.8, $\theta(e)$ = 8 m)

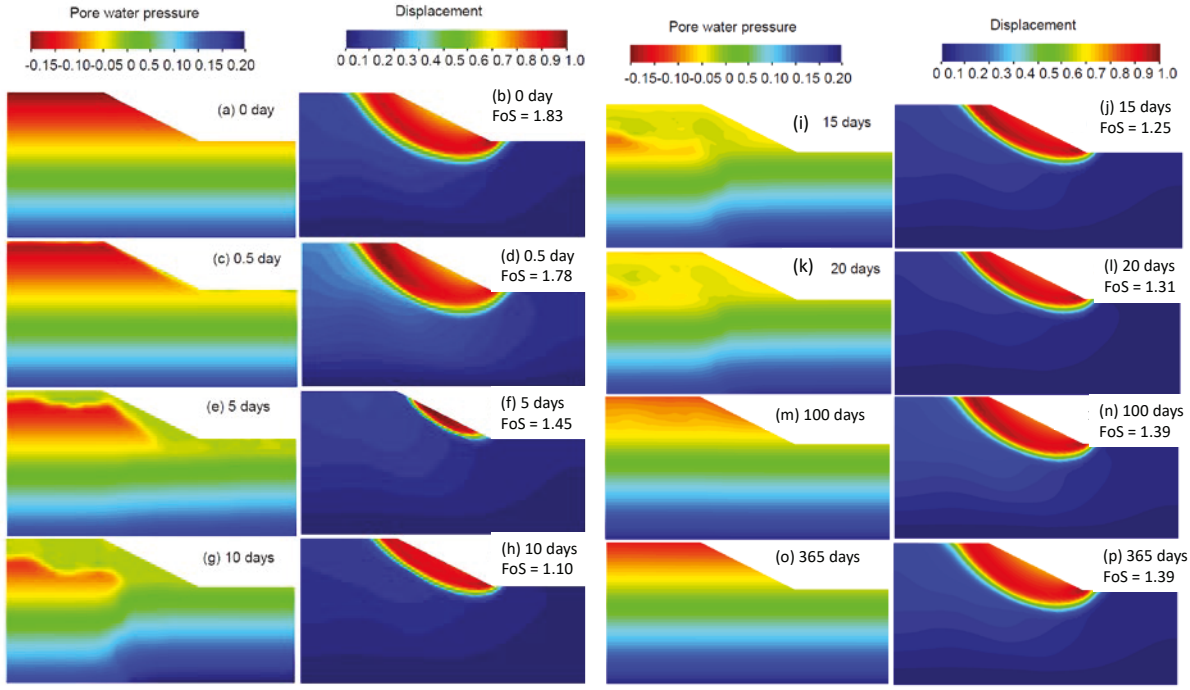

Figure 6: Evolution of pore water pressure contours and slip surfaces at different times during and after the rainfall (corresponding to the porosity distribution in Figure 5, $\mu(e)$ = 0.5, COV_e = 0.8, $\theta(e)$ = 8 m)

3.3 Influence of porosity variability on Factor of Safety

The variation of the $\mu(FoS)$ and COV_{FoS} at various COV_e show very similar patterns over time (Fig. 7). The $\mu(FoS)$ decreases over the rainfall (day 0 to 10). The lowest $\mu(FoS)$ occurs unanimously at 10 days just before then rainfall stops. From day 10 to day 365, infiltration is no longer occurring leading to the recovering of the $\mu(FoS)$ (Fig. 7a). The assumption of impermeable vertical and bottom boundary after the rainfall leading to accumulation of water in the soil domain. Consequently, the FoS long after the rainfall has stopped (i.e. 365 days) is lower than the initial FoS (i.e. 0 day). The COV_{FoS} is almost the same after half a day of rainfall, then increases from day 0.5 to day 5, peak at day 5 for most cases (except COV_e = 0.1). The COV_{FoS} then decrease from day 5 to day 20 and fluctuate within a small range after 20 days (Fig. 7b).

The porosity heterogeneity within the soil domain increase with increasing COV_e leading to the increasing variability in both stresses distribution (induced by soil overburden weight and degree of saturation heterogeneity) and pore water pressure distribution (induced by permeability heterogeneity). The former leads to the differences in $\mu(FoS)$ and COV_{FoS} between different input COV_e at the initial time step because there is no infiltration so far at this point. The latter exacerbates these differences during the rainfall as can be seen, for example, by the wider distances between data points at 5 days (Fig. 7). As the degree of variability becomes higher (i.e. COV_e increases), the lowest values of the FoS tend to become smaller because the "weakest" slip surface can have lower strength. This leads to the slight decreases in $\mu(FoS)$ (except at 100 and 365 days) and the significantly increases in COV_{FoS} over the whole simulation period.

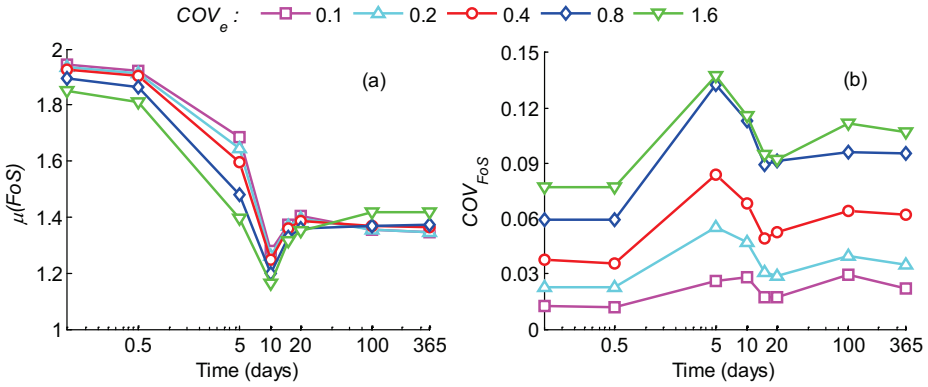

Figure 7: Variation of (a) μ(FoS) and (b) COV_{FoS} of the FoS over time at various COV_e (μ(e) = 0.5, θ(e) = 8 m)

The value of probability of failure (P_f) calculated from the above $\mu(FoS)$ and COV_{FoS} are presented against time and COV_e, assuming a log-normal distribution function governing the FoS data (Fig. 8). The results consistently show the increasing risk of failure with increasing COV_e (Fig. 8). For all the values of COV_e investigated, the P_f generally increases over the rainfall and peaks at 10 days then decreases from 10 days onward (Fig.8a). Some fluctuations at extremely small P_f values causing deviations from this general trend occur early in the rainfall (0.5 days) or close to the end of the simulation period (100 and 365 days). These fluctuations are likely due to the sensitivity of the very small values of P_f to the $\mu(FoS)$ and COV_{FoS}. Note that the vertical axis in Figure 8b has been scaled to limit between 1 and 10^{-12} hence some data points representing $P_f < 10^{-12}$ are not presented in this figure.

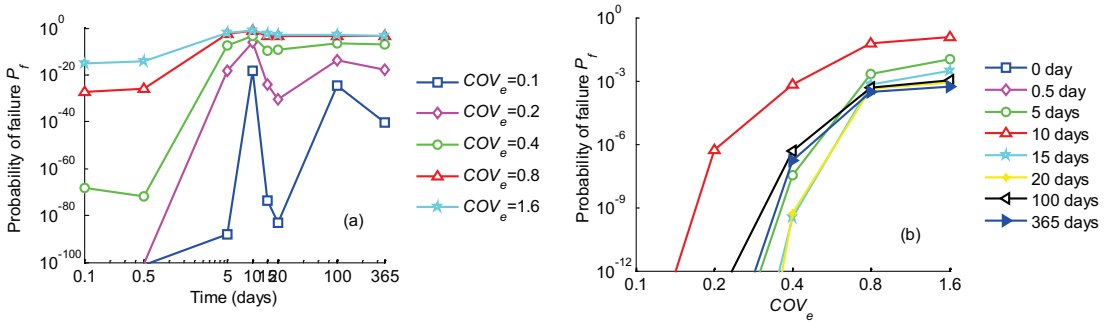

Figure 8: Probability of failure (P_f) against (a) Time (b) Coefficient of variation of void ratio (COV_e)

4 Conclusions

This study has demonstrated the use of probabilistic method to evaluate the factor of safety and probability of failure of a heterogeneous unsaturated slope subjected to rainfall infiltration. It shows that the combination of the finite element method and the random field theory can be powerful and is capable of dealing complex problem which is highly variable in time and space. By using Monte-Carlo analysis, variability of porosity has been shown to significantly influence the mean and coefficient of variation of the factor of safety through its influence on the unsaturated flow. Increasing variability of porosity leads to lower mean value but higher coefficient of variation of the factor of safety. Both of these effects lead to higher probability of failure. Over time, the risk of slope keeps dropping and reaches the lowest at the end of the rainfall, then recovers after the rainfall stops. The study highlights that both time and space are important factors to be taken into account in dealing with wetting of unsaturated slopes.

5 Acknowledgement

The authors gratefully acknowledge the financial support by the Research Council of Norway and several partners through the research Centre SFI Klima 2050 (www.klima2050.no).
i

6 References

[1] Griffiths, D.V. and G.A. Fenton, *Probabilistic Slope Stability Analysis by Finite Elements.* Journal of Geotechnical and Geoenvironmental Engineering, 2004. **130**(5): p. 507-518.

[2] Hicks, M.A. and C. Onisiphorou, *Stochastic evaluation of static liquefaction in a predominantly dilative sand fill.* Géotechnique, 2005. **55**(2): p. 123–133.

[3] Griffiths, D.V. and R.M. Marquez, *Three-dimensional slope stability analysis by elasto-plastic finite elements.* Géotechnique, 2007. **57**(6): p. 537-546.

[4] Griffiths, D.V., J.S. Huang, and G.A. Fenton, *Influence of Spatial Variability on Slope Reliability Using 2-D Random Fields.* Journal of Geotechnical and Geoenvironmental Engineering, 2009. **135**(10): p. 1367-1378.

[5] Hicks, M.A. and K. Samy, *Influence of heterogeneity on undrained clay slope stability.* Quarterly Journal of Engineering Geology and Hydrogeology, 2002. **35**(1): p. 41−49.

[6] Hicks, M.A. and K. Samy. *Influence of anisotropic spatial variability on slope reliability*. in *Proc. 8th Int. Symp. Num. Models Geomech*. 2002. Rome, Italy.

[7] Fenton, G.A. and D.V. Griffiths. *A slope stability reliability model*. in *Proceedings of the K.Y. Lo Symposium*. 2005. London, Ontario.

[8] Hicks, M.A. and W.A. Spencer, *Influence of heterogeneity on the reliability and failure of a long 3D slope.* Computer and Geotechnics, 2010. **37**(7-8): p. 948-955.

[9] Le, T.M.H., et al., *Stability and failure mass of unsaturated heterogeneous slopes.* Canadian Geotechnical Journal, 2015. **52**(11): p. 1747-1761.

[10] Griffiths, D.V. and N. Lu, *Unsaturated slope stability analysis with steady infiltration or evaporation using elasto-plastic finite elements.* International Journal for Numerical and Analytical Methods in Geomechanics, 2005. **29**: p. 249-267.

[11] Lu, N. and J. Godt, *Infinite slope stability under steady unsaturated seepage conditions.* Water Resources Research, 2008. **44**.

[12] Fredlund, D. and H. Rahardjo, *Soil mechanics for unsaturated soils*. 1993, New York: John Wiley & Sons.

[13] Cameron, D.A., et al., *Influence of trees on expansive soils in southern Australia*, in *Expansive soils: recent advances in characterization and treatment*, A.A. Al-Rawas and M.F.A. Goosen, Editors. 2006, Taylor & Francis: London, UK. p. 526.
[14] van Genuchten, M.T., *A closed form equation for predicting the hydraulic conductivity of unsaturated soils.* Soil Science Society of America Journal, 1980. **44**: p. 892-898.
[15] van Genuchten, M.T. and D.R. Nielsen, *On describing and predicting the hydraulic properties of unsaturated soils.* Annales Geophysicae, 1985. **3**(5): p. 615-627.
[16] Fredlund, D.G., N.R. Morgenstern, and R.A. Widger, *The shear strength of an unsaturated soil.* Canadian Geotechnical Journal, 1978. **15**(3): p. 313-321.
[17] Le, T.M.H., *Stochastic Modelling of Slopes and Foundations on Heterogeneous Unsaturated Soils*, in *School of Engineering*. 2011, The University of Glasgow: Glasgow, UK. p. 342.
[18] Le, T.M.H., G. Eiksund, and P.J. Strøm. *Statistical characterisation of soil porosity*. in *Proceeding of the 11th In International Conference on Structural Safety & Reliability*. 2013. Columbia University, New York, USA: CRC Press/Balkema.
[19] Phoon, K. and F. Kulhawy, *Characterization of geotechnical variability.* Canadian Geotechnical Journal, 1999(36): p. 612-624.
[20] Le, T.M.H., et al., *Stochastic analysis of unsaturated seepage through randomly heterogeneous earth embankments.* International Journal for Numerical and Analytical Methods in Geomechanics, 2012. **36**(8): p. 1056-1076.
[21] Le, T.M.H., et al., *Rainfall-induced differential settlements of foundations on heterogeneous unsaturated soils.* Geotechnique, 2013.